TRIBOLOGIA - Finnish Journal of Tribology 3-4 vol 37/2020

https://doi.org/10.30678/fjt.96048

SUOMEN TRIBOLOGIAYHDISTYS RY
THE FINNISH SOCIETY FOR TRIBOLOGY
www.tribologysociety.fi
https://journal.fi/tribologia

Friction and temperature mapping of environmentally acceptable gear oils

Reza Bayat, Arto Lehtovaara

Tribology and Machine Elements, Materials Science and Environmental Engineering, Faculty of Engineering and Natural Sciences, P.O. Box 589, 33014 Tampere University, Tampere, Finland

Corresponding author: Reza Bayat (reza.bayat@tuni.fi)

ABSTRACT

In recent years, environmental issues have raised the demand to protect the environment against the pollution caused by the uncontrolled spillage of lubricating oils. One solution is using Environmentally Acceptable Lubricants (EALs), however, these oils are more expensive than the common mineral oils. The consumers require to test the oil performance using test machines but testing in real machines is costly and time-consuming. Small test machines like ball-on-disc have been previously used for friction mapping and ranking gear oils. In this paper, the friction maps are measured from 0.65 GPa to 1.25 GPa, and temperature maps are devised to experimentally simulate the gear contact along the line of action. Results illustrate that EALs can provide up to 60 % better frictional efficiency that leads to 20 °C cooler oil temperature in high-pressure contacts operating under elastohydrodynamic lubrication (EHL) regime.

Keywords: Elastohydrodynamic lubrication; Environmentally acceptable lubricant; Temperature map; Friction map; Gear oil

1. Introduction

Environmental awareness has grown in recent years, and different industries are changing their values to decrease environmental damages. Lubricant leakage is a source of pollution in the environment that is estimated 40-50% of the 5 million tonnes used lubricant in Europe [1]. Environmentally accepted lubricants (EALs) with low toxicity, and high biodegradability (≥60%) [1], are considerably less harmful to the environment and can be used in environmentally sensitive areas like marine industry and wind turbines. These oils are introduced to the market since the 1970s [2], and still, the oil manufacturers are optimizing their tribological performance.

Ester oils are the most common base oil used for fully formulated EALs. These oils are considerably more expensive than mineral oils. They have lower friction [3–5] and higher thermal conductivity compared to the mineral oil [6]. Their lower friction coefficient signifies less energy loss in the machine components like gears. However, this does not necessarily mean better protection against failure. Understanding oil tribological performance requires further investigations using modeling or testing the oil by different machines. Modeling has been the topic of several studies to investigate the friction [7–11] and temperature variation [12,13] of gears.

For modeling the friction, the most widely used model is the "nonlinear Maxwell" equation proposed by Johnson and Tevaarwerk [14] that is based on Eyring's rheology model. Another model was proposed by Bair that is based on Carreau–Yasuda rheology equation [15]. There have been many debates on the accuracy of these two models [16,17], however, the Eyring model is more commonly implemented thanks to its simplicity and acceptable accuracy [16]. The model proposed by Bair requires more disposable parameters that are difficult to find for industrial oils. With regard to the contact temperature modeling, Archard model [18] has been commonly used, and it is still implemented in the models [3,19]. In this paper, the Eyring model is used for comparing the rheological properties of the oils, and the Archard model is employed for estimating the contact temperature.

The Elastohydrodynamic lubrication (EHL) friction models usually consider a base oil with a known chemical composition, however, fully formulated industrial oils are a mixture of several base oils and additives. Thus, it is more reliable to employ test machines for oils ranking. On the other hand, using real size test machines is costly and time-consuming. Therefore, elaborating less expensive and quicker tests has been the aim of several studies [20–22]. Kleemola and Lehtovaara modeled the gear contact using a twin-disc machine and showed that the shape of the mean friction coefficient curves is similar in both twin-disc machine and gear; however, a difference was observed that

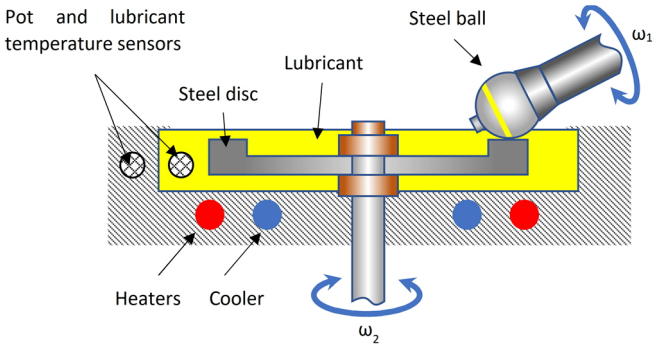

Fig. 1: Schematic of MTM

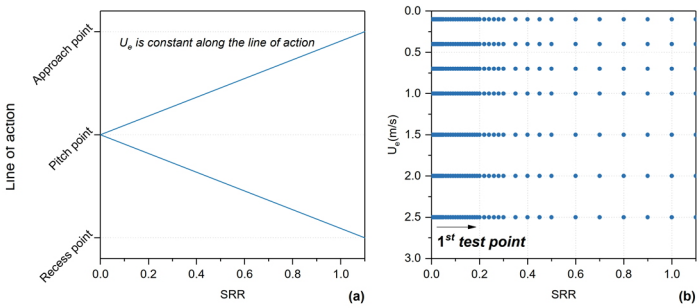

Fig. 2: Estimating friction along the gear line of action: (a) Changes in SRR along the line of action [24]. (b) Test points for measuring the friction and calculating the temperature.

was attributed to the roughness difference between the discs and gear [23]. Björling et. al used a ball-on-disc machine and an FZG machine to rank some oils regarding the friction loss. It was observed that both of the machines give the same ranking [24]. For this ranking, Björling et. al used the friction maps developed earlier in Ref. [25] and estimated the friction at different locations on the line of action of a gear set. This method estimates the variation of friction at different entrainment speeds and sliding-to-rolling ratios (SRRs). The elaborated results can be used for different gear types, and it is not limited to only one specific geometry.

In this paper, the friction mapping method is employed to evaluate the performance of EAL gear oils. In addition, a methodology is devised to plot the temperature maps that show the temperature variation at different working conditions. Firstly, the friction maps are plotted based on the idea of Ref. [24], then using the Archard model, the contact temperature map is plotted by estimating the temperature along the line of action at different entrainment speeds. In order to study the impact of the contact pressures on the EHL friction and temperature, the maps are plotted at four different pressures. This approach graphically represents the interconnection of friction and temperature. Besides, it presents a comparison between frictional and thermal properties of EALs and mineral oils.

2. Experiment detail

The tests were carried out using a mini-traction machine that provided the rolling/sliding contact between a ball and a disc. The tilted ball shaft minimizes the spin, and a load cell attached between the ball shaft and the instrument body measures the friction force. The lubricant and pot temperatures are measured separately and are automatically adjusted by a heater, and a circulating fluid provided by an external heater/cooler equipment. The ball and disc speeds are controlled separately to adjust the oil entrainment speed and sliding-to-rolling ratio (SRR) independently. Entrainment speed and SRR are defined in Eqs. (1)-(3):

$$U_e = \frac{U_d + U_b}{2} \quad (1)$$

$$U_s = U_d - U_b \quad (2)$$

$$SRR = \frac{U_s}{U_e} \quad (3)$$

where U_d and U_b are respectively the disc and ball circumferential velocities in the contact point, U_e is the entrainment velocity and U_s is the sliding velocity.

1.1. Test specimen and lubricants

The ball was manufactured from AISI 52100 steel with a diameter of 19.05 mm, and Rq (Root-Mean-Square roughness) of 50.95 (nm). The disc was from the same material with Rq of 34.08 (nm). Both the ball and disc had the hardness of 750–770 VPN and Young's Modulus of 207 (GPa). For each test, a new ball and disc were cleaned by immersion in toluene and isopropanol in an ultrasonic bath for 10 min.

The tested lubricants include two different EALs with the same viscosity class from different companies and satisfying the US EPA requirements for "Environmentally Acceptable Lubricants". Additionally, two mineral oils were selected for comparison. One mineral gear oil with the same viscosity class, and another mineral engine oil with a similar 40 °C kinematic viscosity that is practically used in ships for gear lubrication. All the oils except M1 that is engine oil, comply with the DIN 51517 part 3 (CLP) standard. The oils specifications can be found in Table 1.

2.1. Friction measurement

Björling et. al explains the correlation between friction at gear contact and a ball on disc machine [24]. In their tested spur gear set with a centre distance of 91.5 mm, gear ratio 1 and normal module 4.5 mm, the SRR varies from 0 to 1.1 at different points along the line of action (Fig. 2 (a)). The SRR represents the position of the point on the line of actions, and the entrainment speed represents the rotational speed of the gear set.

According to the method of Björling et. al [24], the friction was measured in a series of tests at different Ue and SRR. A friction map can be derived by plotting the coefficient of friction (COF) of the measurement points. In this experimental plan, the COF was measured at the data points shown in Fig. 2 (b) covering the whole range of positive SRR.

In order to investigate the effect of pressure, the test was performed at four different maximum Hertzian pressure of 0.65 GPa, 0.95 GPa, 1.10 GPa and 1.25 GPa. The friction map results are shown in Fig. 3-6.

Table 1: Measured lubricants properties

	Kin. Vis. @40 °C (mm²/s)	Kin. Vis. @100 °C (mm²/s)	ρ @15 °C (kg/m³)	VI	Comment
Method	ASTM D445	ASTM D445	EN ISO 12185	ASTM D 2270	
M1	127.60	13.83	908	105	Mineral engine oil
M2	142.50	14.24	888	97	Mineral gear oil
EAL1	147.50	18.84	972	145	Synthetic oil, EAL
EAL2	150.57	18.44	929	137	Synthetic oil, EAL

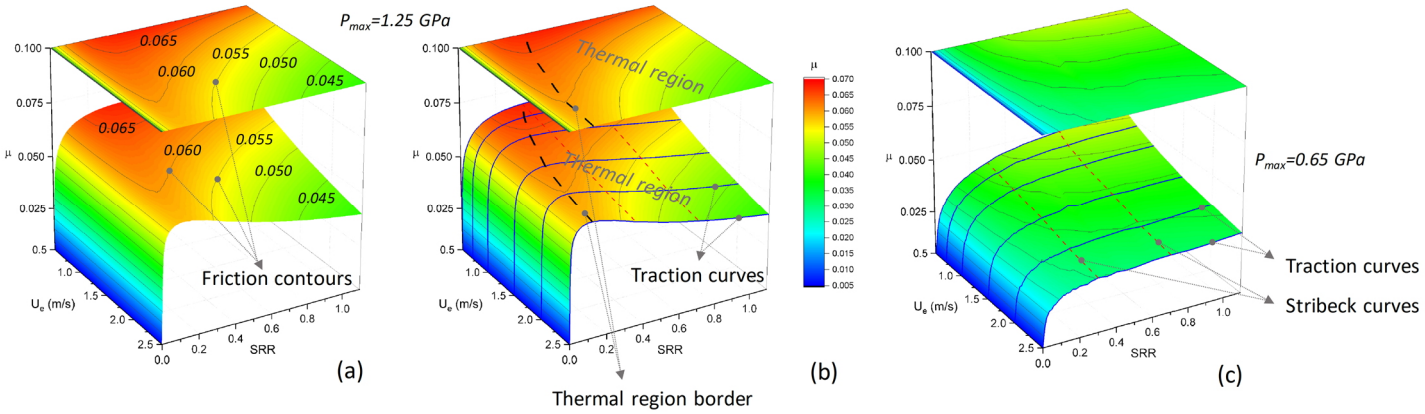

Fig. 3: Extracting 2D friction map from 3D friction map of M1: (a) Friction contours on 2D and 3D friction maps of M1 at P_{max}=1.25, (b) Depiction of the thermal region for M1 at P_{max}=1.25, (c) 2D and 3D friction maps of M1 at P_{max}=0.65, and depiction of traction and stribeck curves

It is noticeable to say that at the entrainment speeds below ~0.5 m/s, the lubrication regime enters to the mixed regime for the used lubricants. Therefore, only the data for the entrainment speeds higher than 0.5 m/s are shown in the friction maps to neglect the effect of asperity contact.

3.1. Temperature calculation

In order to calculate the contact temperature, it is assumed that there is an EHL lubrication regime in the rolling/sliding contact. The heat is generated from shearing and dissipated by conduction in the normal direction, thus there is negligible heat generation by compressive heating or inlet shear heating originated from Poiseuille flow. It is also assumed that the Couette flow is dominant under EHL condition, so the shear strain rate is expressed as:

$$\dot{\gamma} = \frac{U_s}{h_c} \tag{4}$$

By considering the data points that satisfy the specific film thickness values over 3, the contact can be considered as EHL regime that neglects the effect of asperity contact on the friction and heat generation. Considering the aforementioned assumptions, the mean oil film temperature in an EHL increases above the inlet supply temperature by two temperature rise terms: the transient increase in temperature of the contacting surfaces known as the mean flash temperature rise $\Delta\bar{T}_{flash}$, and the second term is the oil film temperature rise above the surfaces denoted by $\Delta\bar{T}_{oil}$. According to Ref. [19], each term can be written as Eqs. 5-7:

$$\bar{T} = T_{supply} + \Delta\bar{T}_{flash} + \Delta\bar{T}_{oil} \tag{5}$$

$$\Delta\bar{T}_{flash} = \frac{1}{(2\pi K\rho c)^{0.5}}\left(\frac{2b}{U_e}\right)^{0.5} q'' \tag{6}$$

$$\Delta\bar{T}_{oil} = \frac{h_c}{8K_{oil}} q'' \tag{7}$$

where K, ρ, and c are respectively the thermal conductivity, density and specific heat of the surfaces (AISI 52100 steel). b is the contact halfwidth and K_{oil} is the oil thermal conductivity. q'' is the rate of heat generation per unit area given by Eq. (8) [19]:

$$q'' = \frac{\mu F U_s}{\pi a^2} = \bar{\tau}\dot{\gamma} h_c \tag{8}$$

where μ is the coefficient of friction (COF), F the normal applied load, $\bar{\tau}$ the mean shear stress calculated by $\bar{\tau} = \frac{F}{\pi a^2}$, $\dot{\gamma}$ the strain rate. h_c is the central film thickness calculated by Hamrock and Dowson's formula [26] and corrected by considering the thermal correction factor presented by Gupta et al. [27]. By using the speed parameter $U = \frac{\eta_0 U_e}{E^* R_x}$, the material parameter $G = \alpha E^*$ and the load parameter $W = \frac{F}{E^* R_x^2}$, the central film thickness can be calculated from Eqs. 9-10:

Table 2: Estimated properties of specimens

	α @40 °C (1/GPa)	Thermal conductivity (W/mK)	Heat capacity (J/kgK)	Density (kg/m³)
Ref.	**[4]**	**[6] for oils, and [19] for ball and disc**	**[19]**	**[19] for ball and disc**
M1	19.95	0.220-0.273	-	Table 1
M2	20.25	0.220-0.273	-	Table 1
EAL1	13.28	0.243-0.295	-	Table 1
EAL2	13.34	0.243-0.295	-	Table 1
Ball and disc AISI 52100 steel	-	21	460	7800

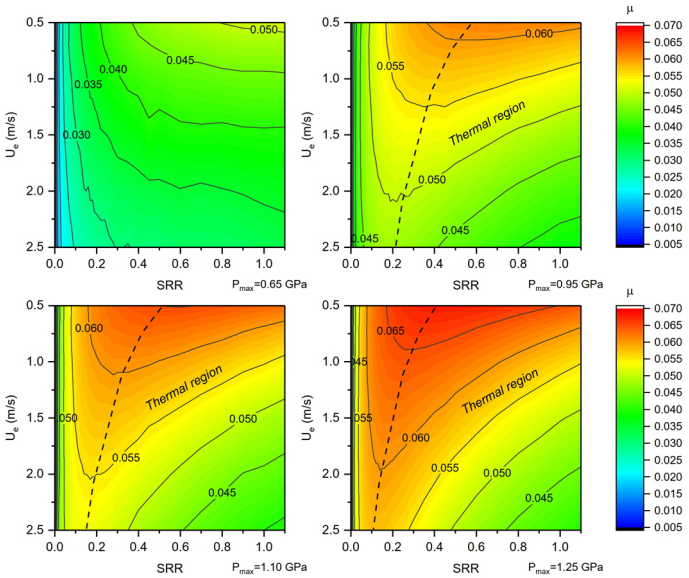

Fig. 4: The COF of M1 at different maximum Hertzian contact pressures

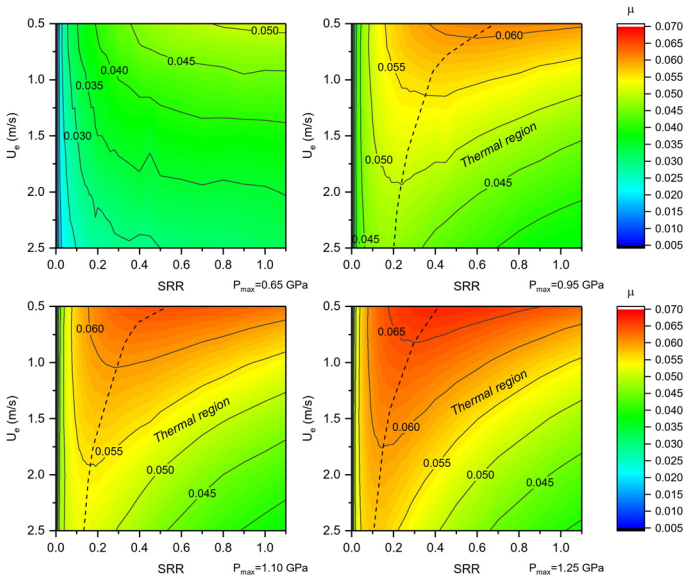

Fig. 5: The COF of M2 at different maximum Hertzian contact pressure

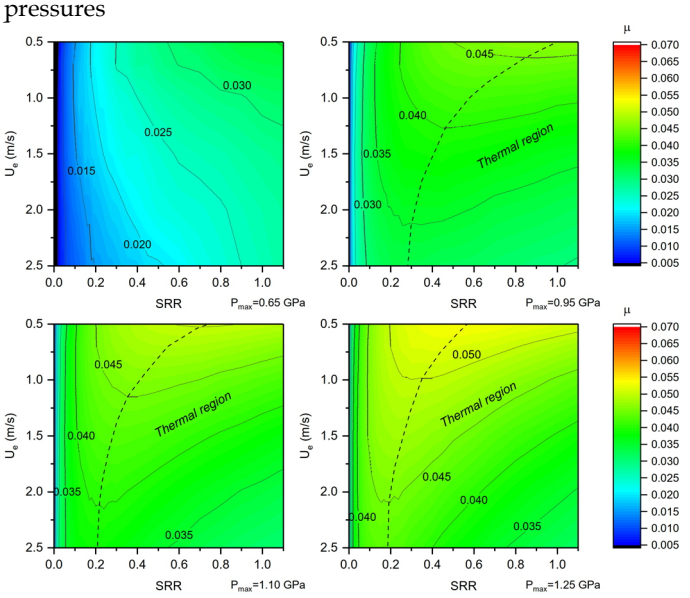

Fig. 6: The COF of EAL1 at different maximum Hertzian contact pressures

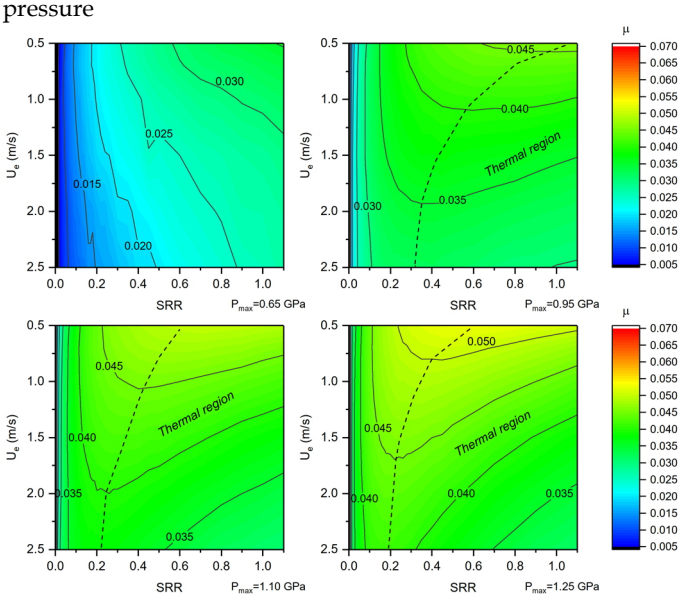

Fig. 7: The COF of EAL2 at different maximum Hertzian contact pressures

$$h_c = h_{c,iso} \cdot \phi_{thermal} \quad (9)$$

$$h_{c,iso} = 2.69R_x(U^{0.67})(G^{0.53})(W^{-0.068})(1-0.61e^{-0.73k}) \quad (10)$$

$$\phi_{thermal} = \frac{1-13.2(p_H/E^*)L^{0.42}}{1+0.213(1+2.23\mathrm{SRR}^{0.83})L^{0.64}} \quad (11)$$

where L is the thermal loading parameter ($L = -\frac{\partial\eta}{\partial T}\frac{u_e^2}{k_{oil}}$), E^* is the reduced Young's Modulus (Pa), R_x the radius of curvature in the x-direction (m), η_0 the dynamic viscosity of the lubricant (Pa s), and $k = 1.03$. The pressure-viscosity coefficient α (Pa^{-1}) was calculated for each pressure using the method presented in Ref. [4].

The film thickness calculation does not consider the shear-thinning effect that leads to overestimation of $\Delta\bar{T}_{oil}$ term. In addition, in this term, the value of 8 in the denominator is based on the assumption that heat is dissipated evenly through the film, and denotes the maximum temperature at the median line of the film [19]. In addition, the thermal conductivity of the oils is estimated based on the data in Ref. [28] by selecting the nearest oil type, and calculating this parameter for each mean contact pressure. The estimated parameters of the samples are shown in Table 2.

For the experimented oils in this study, it is assumed that the contact temperature has a negligible effect on the pressure-viscosity coefficient, thermal conductivity, density and heat capacity.

3. Results and discussion

Figure 3 illustrates the method by which the friction maps are derived. In Fig. 3 (a), a 3D friction map is plotted by evaluating the COF at the data points discussed in section 2.1. Then a 2D friction map is derived by projecting the 3D map to the plane of Ue-SRR while keeping the friction contours and the color variations that illustrate the changes of COF. In Fig. 3 (b), the thermal region and its border are illustrated. According to [14], the thermal region denotes the region in which the shear heating has a dominant effect. Considering a single traction curve in Fig. 3 (b), the thermal region starts from the point at which the COF falls by increasing the SRR. Before the thermal region, there are two other regions: 1) Linear region in which the COF changes linearly with increasing SRR, and 2) non-linear region in which the shear-thinning effect plays its role and leads to a non-linear COF rise [14]. For the case of Fig. 3 (c), no thermal region is observed since the friction does not fall by increasing the SRR. The Hertzian pressure in Fig. 3 (c) is considerably lower than the pressure in Fig. 3 (b), thus it does not lead to a high amount of heat generation.

In addition, the stribeck and traction curves are illustrated in Fig. 3 (c). The traction curves are shown by dark blue solid lines and refer to curves of COF by increasing sliding speed while having a constant entrainment speed. The stribeck curves that are shown by red dash lines, refer to the curves derived from measuring

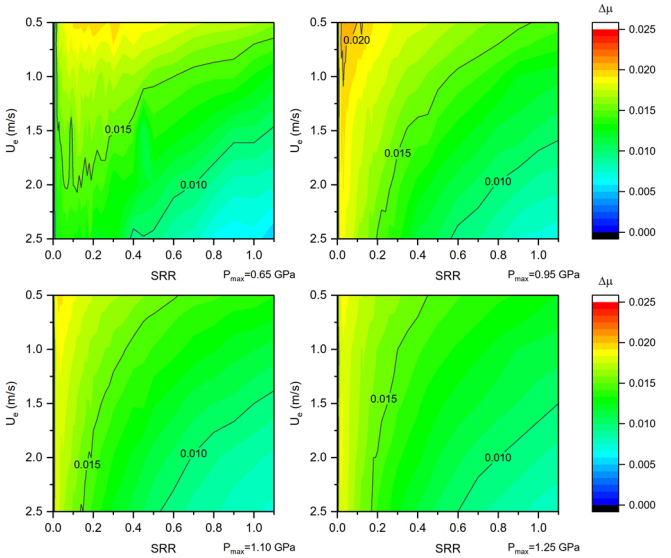

Fig. 8: The difference between COF of M2 and EAL2 at different maximum Hertzian contact pressures

the COF at different entrainment speeds and constant SRR. The traction and stribeck curves of a lubricant can be easily derived for a 2D friction map, at different SRR and entrainment speeds.

The friction maps of the oils are plotted according to the method shown in Fig. 3, then the temperature maps are derived from the friction maps according to the described model. For each oil, the friction and temperature maps are plotted at four different pressures. In these maps, the friction and temperature contours are illustrated, and the thermal regions are shown. It is noticeable that no thermal region was observed in the case of friction maps at the Hertzian pressure of P_{max}=0.65 GPa.

The friction maps of all the oils are shown in Figs. 4-7. For all the cases, by changing the SRR from 0 (pure rolling) to higher values, the friction coefficient first rises and reaches its maximum at the onset of the thermal region. At higher SRRs the heat dissipation becomes effective, and the temperature rises and leads to a reduction of viscosity and lower COF. In conclusion, under the pressures higher than 0.95 GPa, the peak of friction coefficient happens at the regions near the pitch point (low SRR), and the minimum oil viscosity and consequently minimum film thickness is found at the approach or recess points (high SRR).

In Figs. 4-7, in the terms of Stribeck curve at a constant SRR, the increase in entrainment speed leads to lower COF. Since all the friction maps are tested under the EHL regime, the higher entrainment speed at a constant SRR means higher sliding velocity and higher heat generation, thus lowers the oil viscosity and COF.

It can be seen from Figs. 4 and 5 that there is little difference between the COF of two mineral oils. Similarly, this is the case for the EALs (Figs. 6 and 7). Thus, in order to compare the COF of mineral oils with EALs, only one of the mineral oils (M2) was compared with one EAL (EAL2). Figure 8 presents the COF difference between M2 and EAL2 and four different pressures.

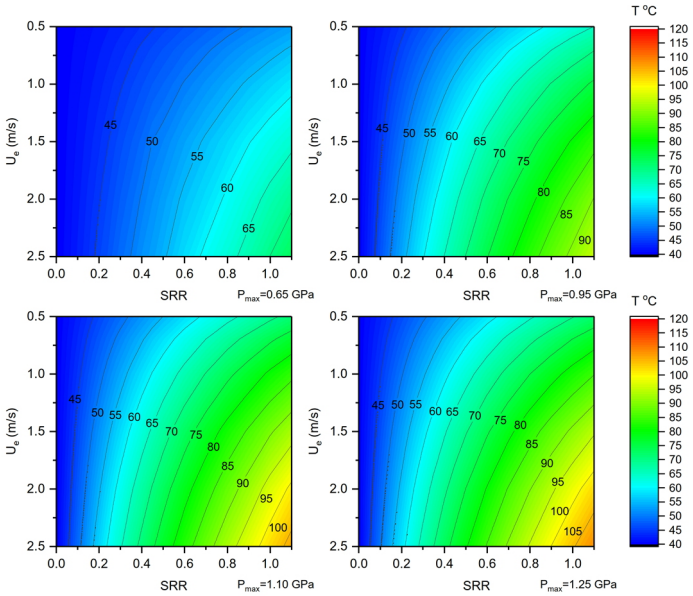

Fig. 9: The Temperature map of M1 at different maximum Hertzian contact pressures

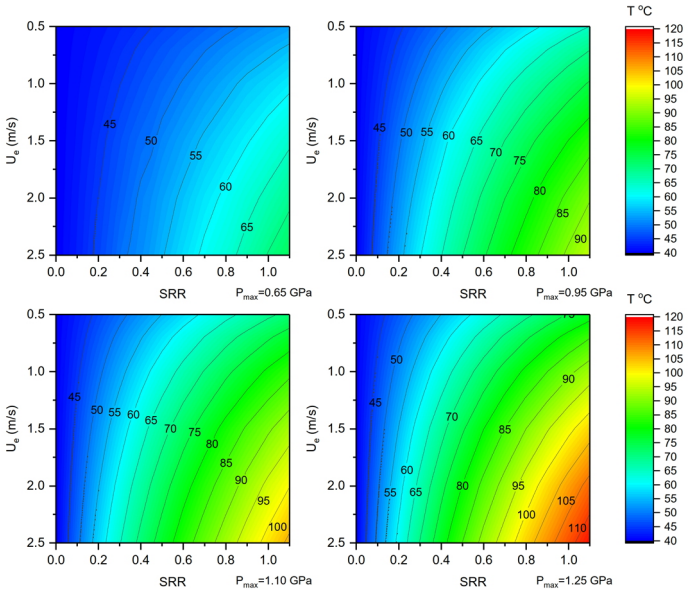

Fig. 10: The Temperature map of M2 at different maximum Hertzian contact pressures

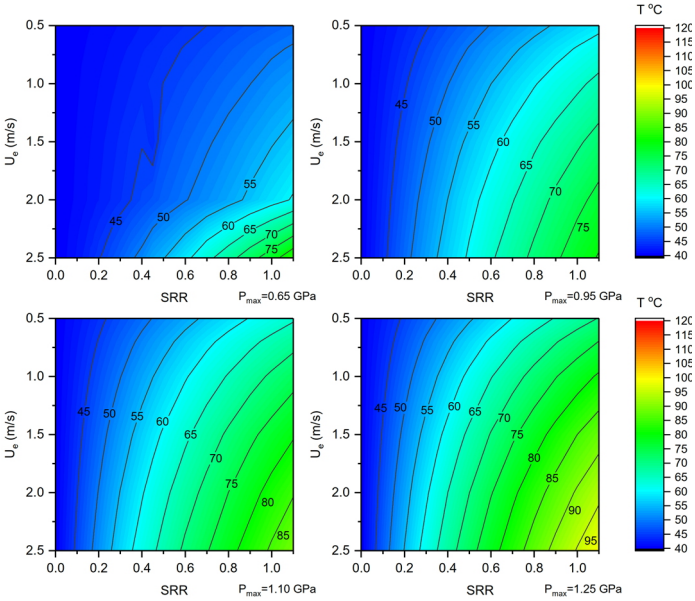

Fig. 11: The Temperature map of EAL1 at different maximum Hertzian contact pressures

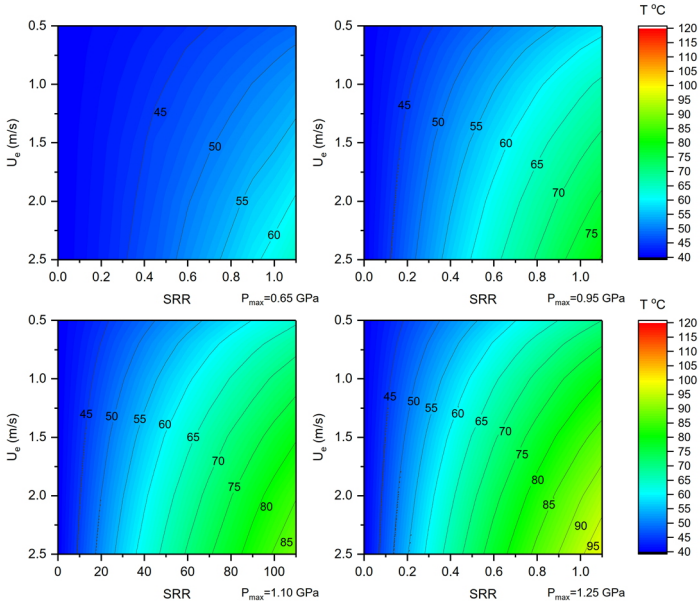

Fig. 12: The Temperature map of EAL2 at different maximum Hertzian contact pressures

Figure 8 shows that the COF decreases by using EALs instead of mineral oils. This reduction is around ~0.02 (60% of mineral oil COF) at low SRR and low Ue, that is the case of roller bearings or regions near the pitch point in gears. However, the COF reduces by ~0.01 (20% of mineral oil COF) at high SRR and high Ue which represents the conditions of the gear tooth tip.

Based on the Eyring stress activation model of isothermal liquid flow, and considering a Barus viscosity-pressure equation, shear stress can be written as Eq. (12) [29]:

$$\tau = \tau_e sinh^{-1}\left(\frac{\eta_0 e^{\alpha p}\dot{\gamma}}{\tau_e}\right) \qquad (12)$$

where τ_e is the limiting stress at which shear-thinning becomes significant, η_0 is the viscosity at atmospheric pressure and α is the pressure-viscosity coefficient.

Using Eq (12), τ_e was estimated for the oils M2 and EAL2 by curve fitting on a plot of τ versus $\dot{\gamma}$. The curve fitting was employed for the traction curve at 40 °C, maximum Hertzian pressure of 1.10 GPa, entrainment speed of 0.7 m/s and considering $\tau > \tau_e$ over most of the contact [30]. The results show that τ_e of M2 was approximately 15 % higher than EAL2. On the other hand, from [31] it is observed that the pressure-viscosity coefficient of EALs is smaller. Therefore, the friction reduction by EALs is mainly attributed to two rheological parameters: the lower pressure-viscosity coefficient of EALs, and their lower limiting shear stress at which shear-thinning becomes

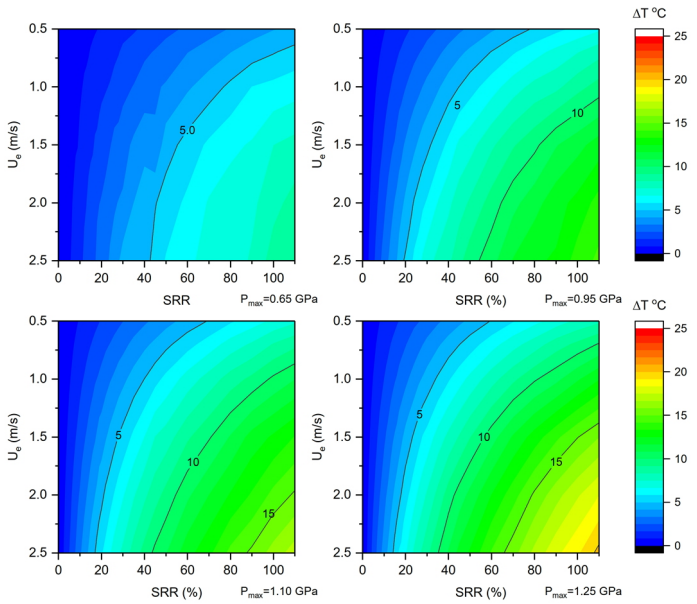

Fig. 13: The difference in temperature of M2 and EAL2 at different maximum Hertzian contact pressures

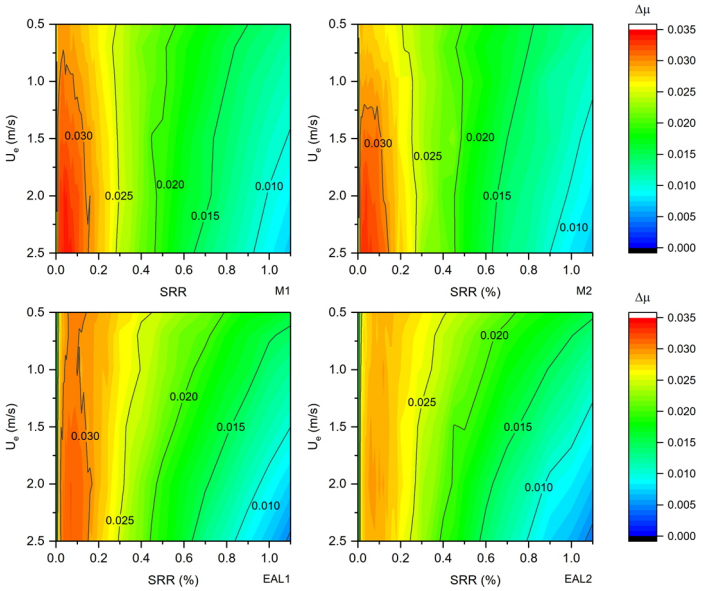

Fig. 14: The difference between COF at P_{max}=0.65 GPa and P_{max}=1.25 GPa for each oil

significant. Regarding the molecular factors contributing to the low COF, Zhang et. al [29] point to the linear chains, flexible groups like C(O)–O–C, and large free volume that reduce the interaction between neighboring molecules.

Figures 9-12 show the temperature maps of the oils at different pressures. Considering the traction curves at a constant entrainment speed, the highest temperature is found at high SRRs, corresponding to the approach or recess points of gear sets. By Increasing the pressure from 0.65 GPa to 1.25 GPa, the maximum temperature of mineral oils increases with the rate of ~77 °C/GPa, while for the case of EALs this rate is ~60 °C/GPa. This lower rate is mainly due to the lower COF and better heat conduction of the oils film in EALs.

In order to compare the temperature of mineral oils with EALs, only one of the mineral oils was compared with one EAL (M2 and EAL2). Figure 13 presents the temperature difference between M2 and EAL2 at four different pressures.

Figure 13 shows that EAL2 has a lower temperature than M2, and their temperature difference ranges from 5 °C at low SRRs, low Ue and low pressure, to 20 °C at high SRR, high Ue and high pressure. According to Eqs. (5)-(7), the lower temperature of EAL2 is a result of its lower COF, and bigger thermal conductivity. By increasing the maximum Hertzian pressure from 0.65 GPa to 1.25 GPa, the temperature difference between these oils grows. This illustrates the higher thermal efficiency of EALs.

In Fig. 13, at low SRRs, the oil temperatures of both oil types show little difference. However, increasing the sliding velocity (high SRR and high Ue) results in a big temperature difference. The high oil film temperature of mineral oils significantly reduces their viscosity which results in decreasing the COF. In Fig. 8, the smaller COF difference at high SRR and high Ue is due to the comparably higher oil film temperature of the mineral oils.

Figure 14 shows that the higher pressure results in COF increase for all the oils that is due to the viscosity increase by pressure. The COF increase is smaller at high SRRs because of the dominance of shear heating. At small SRRs, the COF rise of mineral oils is bigger that can be seen from bigger red areas in mineral oils. This is due to the higher pressure-viscosity coefficient of mineral oils. However, at higher SRRs, the COF rise of mineral oils is smaller that is visible from their larger green and blue area in Fig. 14. This means that the dominance of the temperature rise effect is bigger with the case of mineral oils. In Figs. 4-7, the thermal region shifts to the lower SRR due to increased heat generation by shear stress. It can be seen from Figs. 4-7 that the thermal region starts from lower SRRs for the case of mineral oils signifying the bigger thermal dominance. In conclusion, this variation of COF at different SRRs and Ue suggests that the pressure-viscosity coefficient and limiting shear stress are the effective parameters in the machine elements working at low sliding speeds, while shear heating (or COF) and thermal properties become increasingly effective at high sliding velocities and high pressures.

It should be noted that this study has been primarily concerned with devising a methodology for comparing the industrial EALs with the mineral oils. The friction and temperature values might not be directly transferable to the real machine values. The most important limitation lies in the constant pressure assumed in the current methodology, which is in contradiction with the changing radius and pressure in real gears. Also, in real gear, the surface roughness is higher, which leads to the operation under mixed lubrication regime. In addition, in the temperature model, the mean value is used for different parameters. Also, the effect of the shear-thinning is not considered in calculating the EHL film thickness. Nevertheless, this paper

provides a versatile technique for ranking the oils regarding the contact temperature and friction. This methodology provides a comprehensive analysis of several parameters in a few plots. It can be considered as a quick and preliminary test for estimating the oil performance in different gear types. These data elaborated in this experiment are applicable for any gear set in which the SRR and Ue are in the measured range. In case the gear operates in the higher SRR and Ue, a new friction map can be quickly tested to cover the gear working condition.

Conclusion:

The objective of this work was to examine the friction and temperature of the EALs compared to mineral oils. This was achieved by using a ball on disc test equipment to experimentally simulate gear contact. The friction maps were obtained by evaluating the COF at different entrainment speeds and SRRs. Then, a methodology was devised to plot the temperature maps based on the Archard model. Furthermore, the maps were studied at four different contact pressures to study the impact of pressure on friction and oil temperature. In conclusion, the results of this study show that:

- By using an EAL, the COF in the EHL regime reduced from ~60% at low slide-to-roll ratio (SRR) -low entrainment velocity (Ue), to 20% at high SRR-high Ue.
- The friction reduction by EALs was mainly attributed to two rheological parameters: the lower pressure-viscosity coefficient of EALs, and their lower limiting shear stress.
- At higher pressure, friction increased for all the oils. However, this friction growth was smaller in the thermal region where the oil temperature effect becomes dominant. The dominance of the temperature effect was bigger with the case of mineral oils, and it was observed that their thermal region starts at lower SRRs.
- Comparing the oil film temperature, the EALs showed lower oil temperature. The temperature difference between EALs and the mineral oil ranged from 5 ^{o}C at low SRRs, low Ue and low pressure, to 20 ^{o}C at high SRR, high Ue and high pressure. According to the temperature equation, the lower temperature of EALs was the result of their lower friction and bigger thermal conductivity.
- Pressure had a bigger effect on the temperature of mineral oils. The maximum temperature increased with the rate of ~77 ^{o}C/GPa and ~60 ^{o}C/GPa respectively for mineral oils and EALs. The lower was mainly due to the lower COF and better heat conduction of the oils film in EALs.
- This variation of friction at different SRRs and Ue suggest that the pressure-viscosity coefficient and limiting shear stress are the effective parameters in the machine elements working at low sliding speeds, while, friction coefficient and thermal properties become increasingly effective at high sliding velocities and high pressures.

In this study, the estimated temperature and friction are not necessarily the same as what is found in the gear. This method can be further improved by considering the pressure variation along the line of action, measuring the exact thermal properties of the oils, and using a more accurate temperature model by considering the temperature variation at different points in the contact. However, the temperature maps devised in this study, together with the friction maps, present an estimation of the oil energy efficiency, and can be used in further investigations like studying the scuffing protection of the oils. Knowing the working condition of a gear set, the friction and temperature data, or the method can be used to estimate the friction or temperature.

Acknowledgments

We gratefully acknowledge the financial support from Tampere University graduate school.

References

[1] Luther R. Lubricants in the Environment. In: Mang T, Dresel W, editors. Lubr. Lubr. 3rd ed., Weinheim, Germany: Wiley-VCH Verlag GmbH & Co. KGaA; 2017, p. 153–236. https://doi.org/10.1002/9783527610341.ch7.

[2] Norrby T. Environmentally adapted lubricants – where are the opportunities? Ind Lubr Tribol 2003;55:268–74. https://doi.org/10.1108/00368790310496400.

[3] Kim HM, Spikes H. Correlation of Elastohydrodynamic Friction with Molecular Structure of Highly Refined Hydrocarbon Base Oils. Tribol Lett 2020;68:1–14. https://doi.org/10.1007/s11249-020-1265-5.

[4] Brandão JA, Meheux M, Ville F, Seabra JHO, Castro J. Comparative overview of five gear oils in mixed and boundary film lubrication. Tribol Int 2012;47:50–61. https://doi.org/10.1016/j.triboint.2011.10.007.

[5] Martins R, Seabra J, Brito A, Seyfert C, Luther R, Igartua A. Friction coefficient in FZG gears lubricated with industrial gear oils: Biodegradable ester vs. mineral oil. Tribol Int 2006;39:512–21. https://doi.org/10.1016/J.TRIBOINT.2005.03.021.

[6] Larsson R, Andersson O. Lubricant thermal conductivity and heat capacity under high pressure. Proc Inst Mech Eng Part J J Eng Tribol 2000;214:337–42. https://doi.org/10.1243/1350650001543223.

[7] Martin KF. The efficiency of involute spur gears. J Mech Des Trans ASME 1981;103:160–9. https://doi.org/10.1115/1.3254855.

[8] Hua DY, Khonsari MM. Application of transient elastohydrodynamic lubrication analysis for gear transmissions. Tribol Trans 1995;38:905–13. https://doi.org/10.1080/10402009508983487.

[9] Akbarzadeh S, Khonsari MM. Performance of Spur Gears Considering Surface Roughness and Shear Thinning Lubricant. J Tribol 2008;130:021503.

https://doi.org/10.1115/1.2805431.

[10] Larsson R. Transient non-Newtonian elastohydrodynamic lubrication analysis of an involute spur gear. Wear 1997;207:67–73. https://doi.org/10.1016/S0043-1648(96)07484-4.

[11] Björling M, Habchi W, Bair S, Larsson R, Marklund P. Towards the true prediction of EHL friction. Tribol Int 2013;66:19–26. https://doi.org/10.1016/j.triboint.2013.04.008.

[12] Wang KL, Cheng HS. A numerical solution to the dynamic load, film thickness, and surface temperatures in spur gears, part 1 analysis. J Mech Des Trans ASME 1981;103:177–87. https://doi.org/10.1115/1.3254859.

[13] Akbarzadeh S, Khonsari MM. Thermoelastohydrodynamic analysis of spur gears with consideration of surface roughness. Tribol Lett 2008;32:129–41. https://doi.org/10.1007/s11249-008-9370-x.

[14] Johnson KL, Tevaarwerk JL. Shear Behaviour of Elastohydrodynamic Oil Films. Proc R Soc London Ser A, Math Phys Sci 1977;356:215–36. https://doi.org/10.1098/rspa.1977.0129.

[15] Bair S. "Recent Developments in High-Pressure Rheology of Lubricants". Tribol Ser 1995;30:169–87. https://doi.org/10.1016/S0167-8922(08)70628-X.

[16] Spikes H, Jie Z. History, Origins and Prediction of Elastohydrodynamic Friction. Tribol Lett 2014;56:1–25. https://doi.org/10.1007/s11249-014-0396-y.

[17] Bair S, Vergne P, Kumar P, Poll G, Krupka I, Hartl M, et al. Comment on "History, Origins and Prediction of Elastohydrodynamic Friction" by Spikes and Jie. Tribol Lett 2015;58:1–8. https://doi.org/10.1007/s11249-015-0481-x.

[18] Archard JF. The temperature of rubbing surfaces. Wear 1959;2:438–55. https://doi.org/10.1016/0043-1648(59)90159-0.

[19] Zhang J, Spikes H. Measurement of EHD Friction at Very High Contact Pressures. Tribol Lett 2020;68:1–12. https://doi.org/10.1007/s11249-020-1281-5.

[20] Johnson KL, Spence DI. Determination of gear tooth friction by disc machine. Tribol Int 1991;24:269–75. https://doi.org/10.1016/0301-679X(91)90029-9.

[21] Höhn B-R, Michaelis K, Doleschel A. Frictional behaviour of synthetic gear lubricants. Tribol Ser 2001;39:759–68. https://doi.org/10.1016/S0167-8922(01)80156-5.

[22] Kleemola J, Lehtovaara A. Development of a high pressure twin disc test device for the simulation of gear contact. Tribologia 2006;25:8–17.

[23] Kleemola J, Lehtovaara A. Experimental simulation of gear contact along the line of action. Tribol Int 2009;42:1453–9. https://doi.org/10.1016/J.TRIBOINT.2009.06.007.

[24] Björling M, Miettinen J, Marklund P, Lehtovaara A, Larsson R. The correlation between gear contact friction and ball on disc friction measurements. Tribol Int 2015;83:114–9. https://doi.org/10.1016/j.triboint.2014.11.007.

[25] Björling M, Larsson R, Marklund P, Kassfeldt E. Elastohydrodynamic lubrication friction mapping – the influence of lubricant, roughness, speed, and slide-to-roll ratio. Proc Inst Mech Eng Part J J Eng Tribol 2011;225:671–81. https://doi.org/10.1177/1350650111403363.

[26] Hamrock BJ, Dowson D. Isothermal Elastohydrodynamic Lubrication of Point Contacts: Part III—Fully Flooded Results. J Lubr Technol 1977;99:264–75. https://doi.org/10.1115/1.3453074.

[27] Gupta PK, Cheng HS, Zhu D, Forster NH, Schrand JB. Viscoelastic effects in MIL-L-7808-type lubricant, part I: Analytical formulation. Tribol Trans 1992;35:269–74. https://doi.org/10.1080/10402009208982117.

[28] Larsson R, Larsson PO, Eriksson E, Sjöberg M, Höglund E. Lubricant properties for input to hydrodynamic and elastohydrodynamic lubrication analyses. Proc Inst Mech Eng Part J J Eng Tribol 2000;214:17–27. https://doi.org/10.1243/1350650001542981.

[29] Zhang J, Tan A, Spikes HA. Effect of Base Oil Structure on Elastohydrodynamic Friction. Tribol Lett 2017;65:1–24. https://doi.org/10.1007/s11249-016-0791-7.

[30] Evans CR, Johnson KL. The Rheological Properties of Elastohydrodynamic Lubricants. Proc Inst Mech Eng Part C J Mech Eng Sci 1986;200:303–12. https://doi.org/10.1243/PIME_PROC_1986_200_134_02.

[31] Bayat R, Lehtovaara A. EHL/mixed transition of fully formulated environmentally acceptable gear oils. Tribol Int 2020:106158. https://doi.org/10.1016/j.triboint.2020.106158.